
Variational Wasserstein gradient flow

Jiaojiao Fan

Georgia Institute of Technology
jiaojiaofan@gatech.edu

Amirhossein Taghvaei

University of Washington, Seattle
amirtag@uw.edu

Yongxin Chen

Georgia Institute of Technology
yongchen@gatech.edu

Abstract

The gradient flow of a function over the space of probability densities with respect to the Wasserstein metric often exhibits nice properties and has been utilized in several machine learning applications. The standard approach to compute the Wasserstein gradient flow is the finite difference which discretizes the underlying space over a grid, and is not scalable. In this work, we propose a scalable proximal gradient type algorithm for Wasserstein gradient flow. The key of our method is a variational formulation of the objective function, which makes it possible to realize the JKO proximal map through a primal-dual optimization. This primal-dual problem can be efficiently solved by alternatively updating the parameters in the inner and outer loops. Our framework covers all the classical Wasserstein gradient flows including the heat equation and the porous medium equation. We demonstrate the performance and scalability of our algorithm with several numerical examples.

1 Introduction

The Wasserstein gradient flow models the gradient dynamics over the space of probability densities with respect to the Wasserstein metric. It was first discovered by Jordan, Kinderlehrer, and Otto (JKO) in their seminal work (Jordan et al., 1998). They pointed out that the Fokker-Planck equation is in fact the Wasserstein gradient flow of the free energy, bringing tremendous physical insights to this type of partial differential equations (PDEs). Since then, the Wasserstein gradient flow has played an important role in optimal transport, PDEs, physics, machine learning, and many other areas (Ambrosio et al., 2008; Otto, 2001; Adams et al., 2011; Santambrogio, 2017; Carlier et al., 2017; Frognier & Poggio, 2020).

Despite the abundant theoretical results on the Wasserstein gradient flow established over the past decades (Ambrosio et al., 2008; Santambrogio, 2017), the computation of it remains a challenge. Most existing methods are either based on finite difference of the underlying PDEs or based on finite dimensional optimization; both require discretization of the underlying space (Peyré, 2015; Benamou et al., 2016; Carlier et al., 2017; Li et al., 2020; Carrillo et al., 2021). The computational complexity of these methods scales exponentially as the problem dimension, making them unsuitable for the cases where probability densities over high dimensional spaces are involved.

Our goal is to develop a scalable method to compute the Wasserstein gradient flow without discretizing the underlying space. One target application we are specifically interested in is optimization over the space of probability densities. Many problems such as variational inference can be viewed as special cases of such optimization. We aim to establish a method for this type of optimization that is applicable to a large class of objective functions.

Our algorithm is based on the JKO scheme (Jordan et al., 1998), which is essentially a backward Euler time discretization method for the continuous time Wasserstein gradient flow. In each step of JKO scheme, one needs to find a probability density that minimizes a weighted sum of the Wasserstein distance (square) to the probability density at the previous step and the objective function. We reparametrize this problem in each step so that the optimization variable becomes the optimal transport map from the probability density at the previous step and the one we want to optimize, recasting the problem into a stochastic optimization framework. This transport map can either be modeled by a standard feedback forward network or the gradient of an input convex neural network. The latter is justified by the fact that the optimal transport map for the optimal transport problem with quadratic cost with any marginals is the gradient of a convex function. Another crucial ingredient of our algorithm is a variational form of the objective function leveraging f -divergence, which has been employed in multiple machine learning applications, such as generative models (Nowozin et al., 2016), and Bayesian inference (Wan et al., 2020). The variational form allows the evaluation of the objective with samples and without density estimation. At the end of the algorithm, a sequence of transport maps connecting an initial distribution and the target distribution are obtained. One can then sample from the target distribution by sampling from the initial distribution (often Gaussian) and then propagating these particles through the sequence of transport maps. When the transport map is modeled by the gradient of an input convex neural network, one can evaluate the target density at every point.

Our contributions can be summarized as follows.

- i). We develop a neural network based algorithm to compute Wasserstein gradient flow without spatial discretization. Our algorithm is applicable to any objective function that has a variational representation.
- ii). We specialize our algorithm to three important cases where the objective functions are the Kullback-Leibler divergence, the generalized entropy, and the interaction energy .
- iii). We apply our algorithm to several representative problems including sampling and aggregation-diffusion equation and obtain respectable performance.

Related works: Most existing methods to compute Wasserstein gradient flow are finite difference based (Peyré, 2015; Benamou et al., 2016; Carlier et al., 2017; Li et al., 2020; Carrillo et al., 2021). These methods require spatial discretization and are thus not scalable to high dimensional settings. Salim et al. (2020) analyze the convergence for a forward-backward scheme but leave the implementation of JKO an open question. There is a line of research that uses particle-based method to estimate the Wasserstein gradient flow (Carrillo et al., 2019a; Frogner & Poggio, 2020). In these algorithms, the current density value is often estimated using kernel method whose complexity scales at least quadratically with the number of particles. More recently, several interesting neural network based methods (Mokrov et al., 2021; Alvarez-Melis et al., 2021; Yang et al., 2020; Bunne et al., 2021; Bonet et al., 2021) were proposed for Wasserstein gradient flow. Mokrov et al. (2021) focuses on the special case with Kullback-Leibler divergence as objective function. Alvarez-Melis et al. (2021) uses a density estimation method to evaluate the objective function by back-propagating to the initial distribution, which could become a computational burden when the number of time discretization is large. Yang et al. (2020) is based on a forward Euler time discretization of the Wasserstein gradient flow and is more sensitive to time stepsize. Bunne et al. (2021) utilizes JKO scheme to approximate a population dynamics given an observed trajectory, which finds application in computational biology. Bonet et al. (2021) replaces Wasserstein distance in JKO by sliced alternative but its connection to the original Wasserstein gradient flow remains unclear. Over the past few years, many neural network based algorithms have been proposed to compute optimal transport map or Wasserstein barycenter (Makkuva et al., 2020; Korotin et al., 2021a; Fan et al., 2020; Korotin et al., 2021b). These can be viewed as special cases of Wasserstein gradient flows or optimizations over the space of probability densities.

2 Background

2.1 Optimal transport and Wasserstein distance

Given two probability distributions P, Q over the Euclidean space \mathbb{R}^n with finite second moments, the optimal transport problem with quadratic cost reads

$$\min_{T: T\#P=Q} \int_{\mathbb{R}^n} \|x - T(x)\|_2^2 dP(x), \tag{1}$$

where the minimization is over all the feasible transport maps that transport mass from distribution P to distribution Q . The feasibility is characterized by the pushforward operator (Bogachev, 2007) as $T\#P = Q$. When the initial distribution P admits a density, the above optimal transport problem (1) has a unique solution and it is the gradient of a convex function, that is,

$$T^* = \nabla\varphi$$

for some convex function $\varphi(\cdot) : \mathbb{R}^n \rightarrow \mathbb{R}$. In this paper, we assume probability measures admit densities and use the notation for the measure and the density interchangeably.

The square-root of the minimum transport cost, namely, the minimum of (1), defines a metric on the space of probability distributions known as the Wasserstein-2 distance (Villani, 2003), denoted by $W_2(P, Q)$. The Wasserstein distance has many nice geometrical properties compared with other distances such as L_2 distance for probability distributions, making it a popular choice in applications.

2.2 Wasserstein gradient flow

Given a function $\mathcal{F}(P)$ over the space of probability densities, the Wasserstein gradient flow describes the dynamics of the probability density when it follows the steepest descent direction of the function $\mathcal{F}(P)$ with respect to the Wasserstein metric W_2 . The Wasserstein gradient flow can be explicitly represented by the PDE

$$\frac{\partial P}{\partial t} = \nabla \cdot \left(P \nabla \frac{\delta \mathcal{F}}{\delta P} \right),$$

where $\delta \mathcal{F} / \delta P$ stands for the gradient of the function \mathcal{F} with respect to the standard L_2 metric (Villani, 2003, Ch. 8)

Many important PDEs are the Wasserstein gradient flow for minimizing certain objective functions $\mathcal{F}(P)$. For instance, when \mathcal{F} is the free energy $\mathcal{F}(P) = \int_{\mathbb{R}^n} P(x) \log P(x) dx + \int_{\mathbb{R}^n} V(x) P(x) dx$, the gradient flow is the Fokker-Planck equation (Jordan et al., 1998) $\frac{\partial P}{\partial t} = \nabla \cdot (P \nabla V) + \Delta P$. When \mathcal{F} is the generalized entropy $\mathcal{F}(P) = \frac{1}{m-1} \int_{\mathbb{R}^n} P^m(x) dx$ for some positive number $m > 1$, the gradient flow is the porous medium equation (Otto, 2001; Vázquez, 2007) $\frac{\partial P}{\partial t} = \Delta P^m$.

3 Methods and algorithms

We are interested in solving the optimization problem

$$\min_P \mathcal{F}(P) \tag{2}$$

over the space of probability densities $\mathcal{P}(\mathbb{R}^n)$. In particular, our objective is to develop a particle-based Wasserstein gradient flow algorithm to numerically solve (2).

The objective function $\mathcal{F}(P)$ could exhibit different form depending on the application. In this paper, we present our algorithm for the linear combination of the following three important cases:

Case I The functional is equal to the KL-divergence with respect to a given target distribution Q

$$\mathcal{F}(P) = \mathcal{D}(P||Q) := \int \log \left(\frac{P(x)}{Q(x)} \right) P(x) dx. \tag{3}$$

This is important for the problem of sampling from a target distribution.

Case II The objective functional is equal to the generalized entropy

$$\mathcal{F}(P) = \mathcal{G}(P) := \frac{1}{m-1} \int P^m(x) dx.$$

This case is important for modeling the porous medium.

Case III The objective functional is equal to the interaction energy

$$\mathcal{F}(P) = \mathcal{W}(P) := \int \int W(x-y) P(x) P(y) dx dy, \quad W : \mathbb{R}^n \rightarrow \mathbb{R}.$$

This case is important for modeling the aggregation equation.

These functionals have been widely studied in the Wasserstein gradient flow literature (Carlier et al., 2017; Santambrogio, 2017; Ambrosio et al., 2008) due to their desirable properties. It can be shown that if $\mathcal{F}(P)$ is composed by the above functionals, under proper assumptions, Wasserstein gradient flow associated with $\mathcal{F}(P)$ converges to the unique solution to (2) (Santambrogio, 2017).

In Section 3.1, 3.2, we first assume $\mathcal{F}(P)$ doesn't include interaction energy, and introduce JKO/backward scheme to solve (2). We then add $\mathcal{W}(P)$ into consideration and present a forward-backward scheme in Section 3.3 and close by showing our Algorithm in Section 3.4.

3.1 JKO scheme and reparametrization

To realize the Wasserstein gradient flow, a discretization over time is needed. One such discretization is the famous JKO scheme (Jordan et al., 1998)

$$P_{k+1} = \arg \min_P \frac{1}{2a} W_2^2(P, P_k) + \mathcal{F}(P). \quad (4)$$

This is essentially a backward Euler discretization or a proximal point method with respect to the Wasserstein metric. The solution to (4) converges to the continuous-time Wasserstein gradient flow when the step size $a \rightarrow 0$.

Thanks to Brenier's Theorem (Brenier, 1991), (4) can be recast as an optimization in terms of the transport maps $T : \mathbb{R}^n \rightarrow \mathbb{R}^n$ from P_k to P , i.e., by defining $P = T\#P_k$. The optimal T is the optimal transport map from P_k to $T\#P_k$ and is thus the gradient of a convex function φ . Therefore, in view of the definition of Wasserstein distance (1), Bunne et al. (2021); Mokrov et al. (2021); Alvarez-Melis et al. (2021) propose to reparametrize T as the gradient of Input convex neural network (ICNN) (Amos et al., 2017) and express (4) as

$$P_{k+1} = \nabla\varphi_k\#P_k, \quad \varphi_k = \arg \min_{\varphi \in \text{CVX}} \frac{1}{2a} \int_{\mathbb{R}^n} \|x - \nabla\varphi(x)\|_2^2 dP_k(x) + \mathcal{F}(\nabla\varphi\#P_k), \quad (5)$$

where CVX stands for the space of convex functions. In our method, we extend this idea and propose to reparametrize T alternatively by a residual neural network. With this reparametrization, the JKO step (4) becomes

$$P_{k+1} = T_k\#P_k, \quad T_k = \arg \min_T \frac{1}{2a} \int_{\mathbb{R}^n} \|x - T(x)\|_2^2 dP_k(x) + \mathcal{F}(T\#P_k). \quad (6)$$

We use the preceding two schemes (5) and (6) in our numerical method depending on the application.

3.2 $\mathcal{D}(P\|Q)$ and $\mathcal{G}(P)$ reformulation with variational formula

The main challenge in implementing the JKO scheme is to evaluate the functional $\mathcal{F}(P)$ in terms of samples from P . We achieve this goal by using a variational formulation of \mathcal{F} . In order to do so, we use the notion of f -divergence between the two distributions P and Q :

$$D_f(P\|Q) = \mathbb{E}_Q \left[f \left(\frac{P}{Q} \right) \right] \quad (7)$$

where $f : (0, +\infty) \rightarrow \mathbb{R}$ is a convex function. The f -divergence admits the variational formulation

$$D_f(P\|Q) = \sup_h \mathbb{E}_P[h(X)] - \mathbb{E}_Q[f^*(h(Y))]. \quad (8)$$

where $f^*(y) = \sup_{x \in \mathbb{R}} [xy - f(x)]$ is the convex conjugate of f . The variational form has the special feature that it does not involve the density of P and Q explicitly and can be approximated in terms of samples from P and Q . The functionals $\mathcal{D}(P\|Q)$ and $\mathcal{G}(P)$ can both be expressed as f -divergence.

With the help of the f -divergence variational formula, when $\mathcal{F}(P) = \mathcal{D}(P\|Q)$ or $\mathcal{G}(P)$, the JKO scheme (6) can be equivalently expressed as

$$P_{k+1} = T_k\#P_k, \quad T_k = \arg \min_T \left\{ \frac{1}{2a} \mathbb{E}_{P_k} [\|X - T(X)\|^2] + \sup_h \mathcal{V}(T, h) \right\}. \quad (9)$$

where $\mathcal{V}(T, h) = \mathbb{E}_{P_k}[\mathcal{A}(T, h)] - \mathbb{E}_\Gamma[\mathcal{B}(h)]$, Γ is a user designed distribution which is easy to sample from, and \mathcal{A} and \mathcal{B} are functionals whose form depends on the functional \mathcal{F} . The form of these two functionals for the KL divergence and the generalized entropy appears in Table 1. The details appear in Section 3.2.1 and 3.2.2.

3.2.1 KL divergence

The KL divergence is the special instance of the f -divergence obtained by replacing f with $f_1(x) = x \log x$ in (7)

$$D_{f_1}(P\|Q) = \mathbb{E}_Q \left[\frac{P}{Q} \log \frac{P}{Q} \right] = \mathbb{E}_P \left[\log \frac{P}{Q} \right].$$

Proposition 1. *The variational formulation for $\mathcal{D}(P\|Q)$ reads*

$$D_{f_1}(P\|Q) = 1 + \sup_h \mathbb{E}_P \left[\log h(X) + \log \frac{\mu(X)}{Q(X)} \right] - \mathbb{E}_\mu [h(Z)],$$

where μ is a user designed distribution which is easy to sample from. The optimal function h is equal to the ratio between the densities of $T\sharp P_k$ and μ .

The proof for Proposition 1 can be found in appendix A. It becomes practical when we have only access to un-normalized density of Q , which is the case for the sampling problem. Using this variational form in the JKO scheme (6) yields $P_{k+1} = T_k\sharp P_k$ and

$$T_k = \arg \min_T \max_h \mathbb{E}_{P_k} \left[\frac{1}{2a} \|X - T(X)\|^2 + \log h(T(X)) + \log \frac{\mu(T(X))}{Q(T(X))} \right] - \mathbb{E}_\mu [h(Z)] \quad (10)$$

In practice, we choose $\mu = \mu_k$ adaptively, where μ_k is the Gaussian with the same mean and covariance as P_k . We noticed that this choice improves the numerical stability of the the algorithm.

Table 1: Variational formula for $\mathcal{D}(P\|Q)$ and $\mathcal{G}(P)$

Energy function	$\mathcal{A}(T, h)$	$\mathcal{B}(h)$	Γ
$\int P \log(P/Q) dx$	$\log h(T) + \log \mu(T) - \log Q(T)$	h	Gaussian distribution μ
$\frac{1}{m-1} \int P^m dx$	$\frac{1}{\Omega_k^{m-1}} \cdot \frac{m}{m-1} (h(T))^{m-1}$	$\frac{1}{\Omega_k^{m-1}} h^m$	Uniform distribution Q

3.2.2 Generalized entropy

The generalized entropy can be also represented as f -divergence. In particular, let $f_2(x) = \frac{1}{m-1}(x^m - x)$ and let Q be the uniform distribution on a set which is the superset of the support of density $P(x)$ and has volume Ω . Then

$$D_{f_2}(P\|Q) = \frac{\Omega^{m-1}}{m-1} \int P^m(x) dx - \frac{1}{m-1}.$$

Proposition 2. *The variational formulation for $\mathcal{G}(P)$ reads*

$$\mathcal{G}(P) = \frac{1}{\Omega^{m-1}} \sup_h \left(\mathbb{E}_{P_k} \left[\frac{m}{m-1} h^{m-1}(X) \right] - \mathbb{E}_Q [h^m(Z)] \right). \quad (11)$$

The optimal function h is equal to the ratio between the densities of $T\sharp P_k$ and Q .

The proof for Proposition 2 is postponed to appendix A. Using this in the JKO scheme yields $P_{k+1} = T_k\sharp P_k$, and

$$T_k = \arg \min_T \max_h \frac{1}{2a} \mathbb{E}_{P_k} \|X - T(X)\|^2 + \frac{1}{\Omega_k^{m-1}} \left(\mathbb{E}_{P_k} \left[\frac{m}{m-1} h^{m-1}(X) \right] - \mathbb{E}_Q [h^m(Z)] \right),$$

where Ω_k is the volume of a set large enough to contain the support of $T\sharp P_k$ for any T that is not too far away from the identity map.

Algorithm 1 Primal-dual gradient flow

Input: Objective function $\mathcal{F}(P)$, initial distribution P_0 , step size a , number of JKO steps K , number of outer loop J_1 , number of inner loop J_2 , batch size M .

Initialization: Parameterized T_θ and h_λ

for $k = 1, 2, \dots, K$ **do**

$P_k \leftarrow (I - a\nabla_x(W * P_k))\#P_k$ if $\mathcal{F}(P)$ includes $\mathcal{W}(P)$

$T_\theta \leftarrow T_{k-1}$ if $k > 1$ {// use last iteration T_{k-1} as a warm-up}

for $j_1 = 1, 2, \dots, J_1$ **do**

Sample Y_1, \dots, Y_M from P_k . Sample Z_1, \dots, Z_M from Γ .

for $j_2 = 1, 2, \dots, J_2$ **do**

Apply Adam to λ to maximize $\frac{1}{M} \sum_{i=1}^M [\mathcal{A}(T_\theta, h_\lambda(Y_i)) - \mathcal{B}(h_\lambda(Z_i))]$.

end for

Apply Adam to θ to minimize $\frac{1}{M} \sum_{i=1}^M [\frac{1}{2a} \|Y_i - T_\theta(Y_i)\|^2 + \mathcal{A}(T_\theta, h_\lambda(Y_i))]$.

end for

$T_k \leftarrow T_\theta$

end for

Output: $\{T_k\}_{k=1}^K$

3.3 Forward Backward (FB) scheme

When $\mathcal{F}(P)$ involves the interaction energy $\mathcal{W}(P)$, we add an additional forward step to solve the gradient flow:

$$P_{k+\frac{1}{2}} := (I - a\nabla_x(W * P_k))\#P_k \quad (12)$$

$$P_{k+1} := T_{k+\frac{1}{2}}\#P_{k+\frac{1}{2}}, \quad (13)$$

where I is the identity map, and $T_{k+\frac{1}{2}}$ is defined by replacing k by $k + \frac{1}{2}$ in (9). In other words, the first gradient descent step (12) is a forward discretization of the gradient flow and the second JKO step (13) is a backward discretization. $\nabla_x(W * P)$ can be written as expectation $\mathbb{E}_{y \sim P} \nabla_x(W(x - y))$, thus can also be approximated by samples. Salim et al. (2020) firstly propose this method to solve Wasserstein gradient flow and provide the theoretical convergence analysis. We make this scheme practical by giving a scalable implementation of JKO.

Since $\mathcal{W}(P)$ can be equivalently written as expectation $\mathbb{E}_{x, y \sim P} [W(x - y)]$, there exists another non-forward-backward (non-FB) method, i.e., removing the first step and integrating $\mathcal{W}(P)$ into a single JKO step: $P_{k+1} = T_k\#P_k$ and

$$T_k = \arg \min_T \left\{ \frac{1}{2a} \mathbb{E}_{P_k} \|X - T(X)\|^2 + \mathbb{E}_{X, Y \sim P_k} [W(T(X) - T(Y))] + \sup_h \mathcal{V}(T, h) \right\}.$$

In practice, we observe the FB scheme is more stable and gives more regular results however converge slower than non-FB scheme. The detailed discussion appears in the Appendix C.2, C.3.

Remark 1. *In principle, one can single out $\log(Q)$ term from (10) and perform a similar forward step $P_{k+\frac{1}{2}} = (I - a(\nabla_x Q)/Q)\#P_k$ (Salim et al., 2020), but we don't observe improved performance of doing this in sampling task.*

3.4 Primal-dual algorithm and parametrization of T and h

The two optimization variables T and h in our minimax formulation (9) can be both parameterized by neural networks, denoted by T_θ and h_λ . With this neural network parametrization, we can then solve the problem by iteratively updating T_θ and h_λ . This primal-dual method to solve (2) is depicted in Algorithm 1.

In this work, we implemented two different architectures for the map T . One way is to use a residual neural network to represent T directly, and another way is to parametrize T as the gradient of a ICNN φ . The latter has been widely used in optimal transport (Makkuva et al., 2020; Fan et al., 2020; Korotin et al., 2021b). Note that ICNN could be modified to be strictly convex and if the function φ is strictly convex, the gradient $\nabla\varphi$ is invertible. However, recently several works (Rout et al., 2021; Korotin et al., 2021a) find poor expressiveness of ICNN architecture and also propose to replace the

gradient of ICNN by a neural network. In our experiments, we find that the first parameterization gives more regular results, which aligns with the result in Bonet et al. (2021, Figure 4). However, it would be very difficult to calculate the density of pushforward distribution. Therefore, with the first parametrization, our method becomes a particle-based method, i.e. we cannot query density directly. As we discuss in Section B, when density evaluation is needed, we adopt the ICNN parameterization since we need to compute T^{-1} .

3.5 Computational complexity

Per each update k in Algorithm 1, the forward step (12) requires at most $O(N^2)$ where N is the total number of particles to push-forward. The backward step (13) requires $O(J_1 k M H)$ where J_1 is the number of iterations per each JKO step, M is the batch size, and H is the size of the network. k shows up in the bound because sampling P_k requires us to pushforward $x_0 \sim P_0$ through $k - 1$ maps.

However, Mokrov et al. (2021) requires $O(J_1((k+n)MH+n^3))$ which has the cubic dependence on dimension n because they need to query the $\log \det \nabla^2 \varphi$ in each iteration. We refer to Mokrov et al. (2021, Section 5) for the complexity details of calculating the Hessian term. There exists fast approximation (Huang et al., 2020) of $\log \det \nabla^2 \varphi$ and its gradient using Stochastic Lanczos Quadrature (Ubaru et al., 2017) and Hutchinson trace estimator (Hutchinson, 1989). Alvarez-Melis et al. (2021) applies this, thus the cubic dependence on n can be improved to quadratic dependence. Nonetheless, this is accompanied by an additional cost, which is the number of iterations to run conjugate gradient (CG) method. CG is guaranteed to converge exactly in n steps in this setting. If one wants to obtain $\log \det \nabla^2 \varphi$ precisely, the cost is still $O(n^3)$, which is the same as calculating $\log \det \nabla^2 \varphi$ directly. If one uses an error ϵ stopping condition in CG, the complexity could be improved to $\sqrt{\kappa} \log(2/\epsilon) n^2$, where κ is the conditional number of $\nabla^2 \varphi$, but this would sacrifice on the accuracy. Thus our method has the advantage of independence on the dimension.

We provide training time details in Section 4.2 and Appendix C.4. Other than training and sampling time, the complexity for evaluating the density are the same as the above two methods due to the standard density evaluation process (see Section B).

4 Numerical examples

4.1 Sampling

We first consider the sampling problem to sample from a target distribution Q . Note that Q doesn't have to be normalized. To this end, we consider the Wasserstein gradient flow with objective function $\mathcal{F}(P) = \int P \log(P/Q) dx$, that is, the KL divergence between distributions P and Q . When this objective is minimized, $P \propto Q$. In our experiments, we consider two types of target distribution: the two moons distribution and the Gaussian mixture model (GMM) with spherical Gaussian components. In this set of experiments, the step size is set to be $a = 0.3$ and the initial measure is a spherical Gaussian $\mathcal{N}(0, 2.25I_d)$.

Two moons: The two moons distribution is a popular target distribution for sampling task. It is a 2D mixture model composed of 16 Gaussian components; each moon shape consists of 8 Gaussian components. The results are displayed in Figure 1, from which we see that our method is able to generate samples that match the target distribution.

GMM with spherical Gaussians: We also test our algorithm in sampling from GMM in higher dimensional space. The target GMM has 9 Gaussian components with equal weights and the same covariances. The results with dimension $n = 8$ and $n = 13$ are depicted in Figure 2. In Figure 2, we not only display the samples as grey dots in the plot, but also the kernel density estimation of generated samples as level sets. As can be seen from the results, both the samples and densities obtained with our algorithm match the target distribution well.

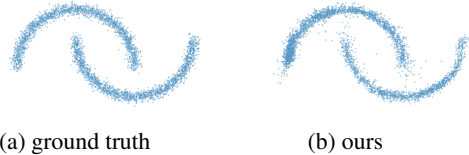


Figure 1: The left figure shows samples from the target 16-GMM distribution and the right figure shows samples obtained by our method. Each plot contains 4000 points.

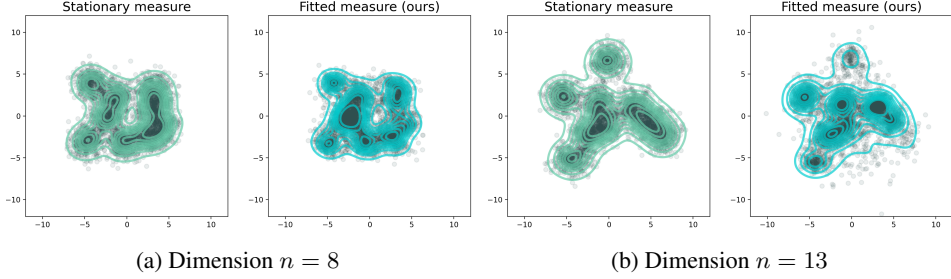


Figure 2: Comparison between the target GMM and fitted measure of generated samples by our method. Samples are projected onto 2D plane by performing PCA. We refer the reader to Mokrov et al. (2021) for the performance of another algorithm in similar setup.

4.2 Ornstein-Uhlenbeck Process

We study the performance of our method in modeling the Ornstein-Uhlenbeck Process as dimension grows. The gradient flow is affiliated with the free energy (3), where $Q = e^{(x-b)^T A(x-b)/2}$ with a positive definite matrix $A \in \mathbb{R}^n \times \mathbb{R}^n$ and $b \in \mathbb{R}^n$. Given an initial Gaussian distribution $\mathcal{N}(0, I_n)$, the gradient flow at each time t is a Gaussian distribution P_t with mean vector $\mu_t = (I_n - e^{-At})b$ and covariance $\Sigma_t = A^{-1}(I_n - e^{-2At}) + e^{-2At}$ (Vatiwutipong & Phewchean, 2019). We calculate P_k with JKO step size $a = 0.05$ and compare with the Fokker-Planck (FP) JKO (Mokrov et al., 2021). We quantify the error as the SymKL divergence between estimated distribution and the ground truth in Figure 3, where

$$\text{SymKL}(P_1, P_2) := D(P_1 \| P_2) + D(P_2 \| P_1).$$

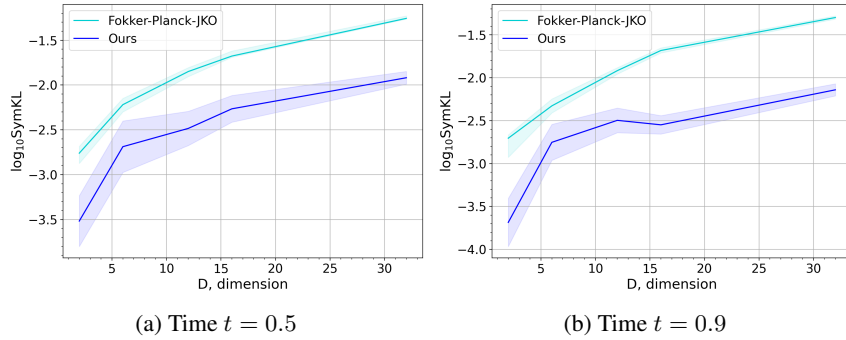


Figure 3: We repeat the experiments for 15 times in dimensions $d = 2, 6, 12, 16, 32$.

We believe that there are several reasons we have better performance. 1) The proposed distribution μ is Gaussian, which is consistent with P_t for any t . This is beneficial for the inner maximization to find a precise h . 2) The map T is linear, so it can promise our generated samples are always from a Gaussian distribution. Note that if one approximate map as gradient of ICNN, it's not guaranteed that the mapped distribution is still Gaussian. We also compare the training time per every two JKO steps with FP JKO. The computation time for FP JKO is around 20s when $d = 2$ and increases to 100s when $d = 32$. Our method's training time remains at $20s \pm 2s$ for all the dimensions $d = 2 \sim 32$. This is due to we fix the neural network size for both methods and our method's computation complexity doesn't depend on the dimension.

4.3 Porous media equation

We next consider the porous media equation with only diffusion: $\partial_t P = \Delta P^m$. This is the Wasserstein gradient flow associated with the energy function $\mathcal{F}(P) = \frac{1}{m-1} \int P^m(x) dx$. A representative

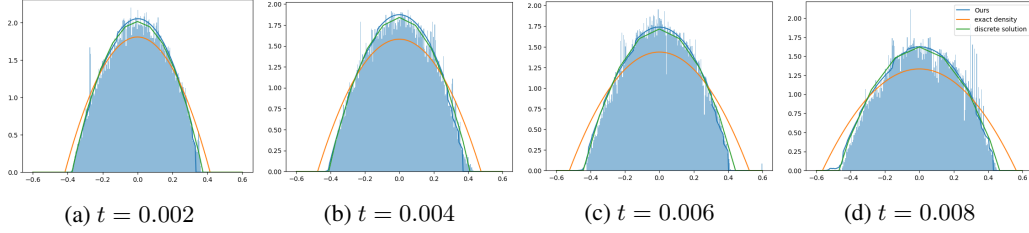


Figure 4: Comparison among exact density, finite difference method solution given by CVXOPT, and the density given by our method. To better visualize the distributed particles from each distribution, we also plot the histograms of our method as the blue shadow.

closed-form solution of the porous media equation is the Barenblatt profile (GI, 1952; Vázquez, 2007)

$$P_{gt}(t, x) = (t + t_0)^{-\alpha} \left(C - \beta (x - x_0)^2 (t + t_0)^{-2\alpha/n} \right)_+^{\frac{1}{m-1}},$$

where $\alpha = \frac{n}{n(m-1) + 2}$, $\beta = \frac{(m-1)\alpha}{2mn}$,

and $t_0 > 0$ is the starting time and $C > 0$ is a free parameter.

In principle, our algorithm should match the analytical solution P_{gt} when the step size a is sufficiently small. When a is not that small, time discretization is inevitable. To account for the time-discretization error of JKO scheme, we consider the porous media equation in 1D space and use the solution via finite difference method as a reference. The details appear in appendix D.3.

In the experiments, we set the stepsize for the JKO scheme to be $a = 0.001$ and the initial time to be $t_0 = 0.002$. Other parameters are chosen as $C = (3/16)^{1/3}$, $m = 2$, $n = 1$, $d = 300$. We parametrize the transport map T as the gradient of an ICNN and thus we can evaluate the density following Section B. In Figure 4, we observe that the gap between the density computed using our algorithm and the ground truth density P_{gt} is dominated by the time-discretization error of the JKO scheme. Our result matches the discrete time solution nicely.

4.4 Aggregation–Diffusion Equation

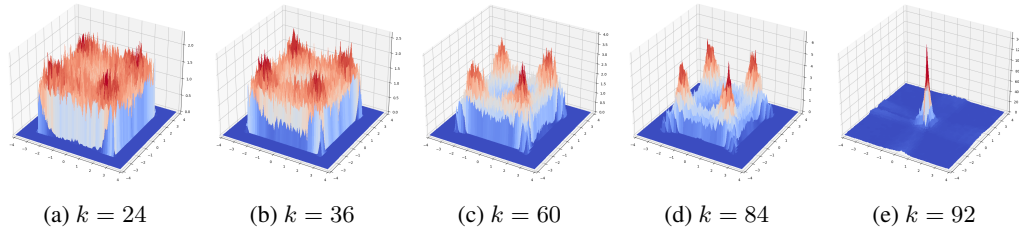


Figure 5: Histogram for simulated measures P_k by FB scheme at different k .

We finally simulate the evolution of solutions to the following aggregation-diffusion equation:

$$\partial_t P = \nabla \cdot (P \nabla W * P) + 0.1 \Delta P^m, \quad W(x) = -e^{-\|x\|^2} / \pi.$$

This corresponds to the energy function $\mathcal{W}(P) + 0.1 \mathcal{G}(P)$. We use the same parameters in Carrillo et al. (2021, Section 4.3.3). The initial distribution is a uniform distribution supported on $[-3, 3] \times [-3, 3]$ and the JKO step size $a = 0.5$. In Figure 5, we utilize FB scheme to simulate the gradient flow for this equation with $m = 3$ on \mathbb{R}^2 space. With this choice $W(x)$, $\nabla_x (W * P_k)$ is equal to $\mathbb{E}_{y \sim P_k} [2e^{-\|x-y\|^2} / \pi]$ in the gradient descent step (12). And we estimate $\nabla_x (W * P_k)$ with 10^4 samples from P_k .

Throughout the process, the aggregation term $\nabla \cdot (P \nabla W * P)$ and the diffusion $0.1 \Delta P^m$ adversarially exert their effects and cause the probability measure split for four pulses and converge to a single pulse in the end (Carrillo et al., 2019b).

5 Conclusion

In this paper we presented a novel neural network based algorithm to compute the Wasserstein gradient flow. Our algorithm follows the JKO time discretization scheme. We reparametrize the problem so that the optimization variable becomes the transport map T between the consecutive steps. By utilizing a variational formula of the objective function, we further reformulate the problem in every step as a min-max problem over map T and dual function h respectively. This formulation doesn't require density estimation using samples and can be optimized using stochastic optimization. It also shows advantages with dimension-independent computation complexity. Our method can also be extended to minimize other objective functions that can be written as f -divergence. Our limitation is the accuracy is not satisfying in sampling tasks with high dimension complex density.

References

- Adams, S., Dirr, N., Peletier, M. A., and Zimmer, J. From a large-deviations principle to the Wasserstein gradient flow: a new micro-macro passage. *Communications in Mathematical Physics*, 307(3):791–815, 2011.
- Alvarez-Melis, D., Schiff, Y., and Mroueh, Y. Optimizing functionals on the space of probabilities with input convex neural networks. *arXiv preprint arXiv:2106.00774*, 2021.
- Ambrosio, L., Gigli, N., and Savaré, G. *Gradient flows: in metric spaces and in the space of probability measures*. Springer Science & Business Media, 2008.
- Amos, B., Xu, L., and Kolter, J. Z. Input convex neural networks. In *International Conference on Machine Learning*, pp. 146–155. PMLR, 2017.
- Benamou, J.-D., Carlier, G., Mérigot, Q., and Oudet, E. Discretization of functionals involving the monge–ampère operator. *Numerische mathematik*, 134(3):611–636, 2016.
- Bogachev, V. I. *Measure theory*, volume 1. Springer Science & Business Media, 2007.
- Bonet, C., Courty, N., Septier, F., and Drumetz, L. Sliced-wasserstein gradient flows. *arXiv preprint arXiv:2110.10972*, 2021.
- Brenier, Y. Polar factorization and monotone rearrangement of vector-valued functions. *Communications on pure and applied mathematics*, 44(4):375–417, 1991.
- Bunne, C., Meng-Papaxanthos, L., Krause, A., and Cuturi, M. Jkonet: Proximal optimal transport modeling of population dynamics. *arXiv preprint arXiv:2106.06345*, 2021.
- Carlier, G., Duval, V., Peyré, G., and Schmitzer, B. Convergence of entropic schemes for optimal transport and gradient flows. *SIAM Journal on Mathematical Analysis*, 49(2):1385–1418, 2017.
- Carrillo, J. A., Craig, K., and Patacchini, F. S. A blob method for diffusion. *Calculus of Variations and Partial Differential Equations*, 58(2):1–53, 2019a.
- Carrillo, J. A., Hittmeir, S., Volzone, B., and Yao, Y. Nonlinear aggregation-diffusion equations: radial symmetry and long time asymptotics. *Inventiones mathematicae*, 218(3):889–977, 2019b.
- Carrillo, J. A., Craig, K., Wang, L., and Wei, C. Primal dual methods for Wasserstein gradient flows. *Foundations of Computational Mathematics*, pp. 1–55, 2021.
- Falcon, W. and Cho, K. A framework for contrastive self-supervised learning and designing a new approach. *arXiv preprint arXiv:2009.00104*, 2020.
- Fan, J., Taghvaei, A., and Chen, Y. Scalable computations of Wasserstein barycenter via input convex neural networks. *arXiv preprint arXiv:2007.04462*, 2020.
- Frogner, C. and Poggio, T. Approximate inference with Wasserstein gradient flows. In *International Conference on Artificial Intelligence and Statistics*, pp. 2581–2590. PMLR, 2020.
- GI, B. On some unsteady motions of a liquid and gas in a porous medium. *Prikl. Mat. Mekh.*, 16: 67–78, 1952.
- Huang, C.-W., Chen, R. T., Tsigotis, C., and Courville, A. Convex potential flows: Universal probability distributions with optimal transport and convex optimization. *arXiv preprint arXiv:2012.05942*, 2020.
- Hutchinson, M. F. A stochastic estimator of the trace of the influence matrix for laplacian smoothing splines. *Communications in Statistics-Simulation and Computation*, 18(3):1059–1076, 1989.
- Jordan, R., Kinderlehrer, D., and Otto, F. The variational formulation of the Fokker–Planck equation. *SIAM journal on mathematical analysis*, 29(1):1–17, 1998.
- Korotin, A., Egiazarian, V., Asadulaev, A., Safin, A., and Burnaev, E. Wasserstein-2 generative networks. In *International Conference on Learning Representations*, 2021a. URL https://openreview.net/forum?id=bEoxzW_EXsa.

- Korotin, A., Li, L., Solomon, J., and Burnaev, E. Continuous Wasserstein-2 barycenter estimation without minimax optimization. *arXiv preprint arXiv:2102.01752*, 2021b.
- Li, W., Lu, J., and Wang, L. Fisher information regularization schemes for Wasserstein gradient flows. *Journal of Computational Physics*, 416:109449, 2020.
- Makkuva, A., Taghvaei, A., Oh, S., and Lee, J. Optimal transport mapping via input convex neural networks. In *International Conference on Machine Learning*, pp. 6672–6681. PMLR, 2020.
- Mokrov, P., Korotin, A., Li, L., Genevay, A., Solomon, J., and Burnaev, E. Large-scale wasserstein gradient flows. In *Thirty-Fifth Conference on Neural Information Processing Systems*, 2021. URL <https://openreview.net/forum?id=nLLjIuHsMHP>.
- Nowozin, S., Cseke, B., and Tomioka, R. f-gan: Training generative neural samplers using variational divergence minimization. In *Proceedings of the 30th International Conference on Neural Information Processing Systems*, pp. 271–279, 2016.
- Otto, F. The geometry of dissipative evolution equations: the porous medium equation. 2001.
- Peyré, G. Entropic approximation of Wasserstein gradient flows. *SIAM Journal on Imaging Sciences*, 8(4):2323–2351, 2015.
- Rout, L., Korotin, A., and Burnaev, E. Generative modeling with optimal transport maps. *arXiv preprint arXiv:2110.02999*, 2021.
- Salim, A., Korba, A., and Luise, G. The Wasserstein proximal gradient algorithm. *arXiv preprint arXiv:2002.03035*, 2020.
- Santambrogio, F. Euclidean, metric, and wasserstein gradient flows: an overview. *Bulletin of Mathematical Sciences*, 7(1):87–154, 2017.
- Ubaru, S., Chen, J., and Saad, Y. Fast estimation of $\text{tr}(f(a))$ via stochastic lanczos quadrature. *SIAM Journal on Matrix Analysis and Applications*, 38(4):1075–1099, 2017.
- Vatiwutipong, P. and Phewchean, N. Alternative way to derive the distribution of the multivariate ornstein–uhlenbeck process. *Advances in Difference Equations*, 2019(1):1–7, 2019.
- Vázquez, J. L. *The porous medium equation: mathematical theory*. Oxford University Press on Demand, 2007.
- Villani, C. *Topics in optimal transportation*. Number 58. American Mathematical Soc., 2003.
- Wan, N., Li, D., and Hovakimyan, N. f-divergence variational inference. *Advances in Neural Information Processing Systems*, 33, 2020.
- Yang, Z., Zhang, Y., Chen, Y., and Wang, Z. Variational transport: A convergent particle-based algorithm for distributional optimization. *arXiv preprint arXiv:2012.11554*, 2020.

A Details about variational formula in Section 3.2

A.1 KL divergence

The KL divergence is the special instance of the f -divergence obtained by replacing f with $f_1(x) = x \log x$ in (7)

$$D_{f_1}(P\|Q) = \mathbb{E}_Q \left[\frac{P}{Q} \log \frac{P}{Q} \right] = \mathbb{E}_P \left[\log \frac{P}{Q} \right],$$

which, according to (8), admits the variational formulation

$$D_{f_1}(P\|Q) = 1 + \sup_h \mathbb{E}_P [h(X)] - \mathbb{E}_Q [e^{h(Y)}] \quad (14)$$

where the convex conjugate $f_1^*(y) = e^{y-1}$ is used.

The variational formulation can be approximated in terms of samples from P and Q . For the case where we have only access to un-normalized density of Q , which is the case for the sampling problem, we use the following change of variable: $h \rightarrow \log(h) + \log(\mu) - \log(Q)$ where μ is a user designed distribution which is easy to sample from. Under such a change of variable, the variational formulation reads

$$D_{f_1}(P\|Q) = 1 + \sup_h \mathbb{E}_P \left[\log h(X) + \log \frac{\mu(X)}{Q(X)} \right] - \mathbb{E}_\mu [h(Z)].$$

Note that the optimal function h is equal to the ratio between the densities of $T_{\#}^k P_k$ and μ .

Remark 2. *The Donsker-Varadhan formula*

$$\mathcal{D}(P\|Q) = \sup_h \mathbb{E}_P [h(X)] - \log \mathbb{E}_Q [e^{h(Z)}]$$

is another variational representation of KL divergence and it's stronger than (14) because it's an upper bound of (14) for any fixed h . However, we cannot get an unbiased estimation of the objective using samples.

A.2 Generalized entropy

The generalized entropy can be also represented as f -divergence. In particular, let $f_2(x) = \frac{1}{m-1}(x^m - x)$ and let Q be the uniform distribution on a set which is the superset of the support of density $P(x)$ and has volume Ω . Then

$$D_{f_2}(P\|Q) = \frac{\Omega^{m-1}}{m-1} \int P^m(x) dx - \frac{1}{m-1}.$$

As a result, the generalized entropy can be expressed in terms of f -divergence according to

$$\mathcal{G}(P) = \frac{1}{m-1} \int P^m(x) dx = \frac{1}{\Omega^{m-1}} D_{f_2}(P\|Q) + \frac{1}{\Omega^{m-1}(m-1)}.$$

Upon using the variational representation of the f -divergence with

$$f_2^*(y) = \left(\frac{(m-1)y + 1}{m} \right)^{\frac{m}{m-1}},$$

the generalized entropy admits the following variational formulation

$$\mathcal{G}(P) = \sup_h \frac{1}{\Omega^{m-1}} \left(\mathbb{E}_P [h(X)] - \mathbb{E}_Q \left[\left(\frac{(m-1)h(Y) + 1}{m} \right)^{\frac{m}{m-1}} \right] \right) + \frac{1}{\Omega^{m-1}(m-1)}.$$

In practice, we find it numerically useful to let $h = \frac{1}{m-1} \left[m (\hat{h})^{m-1} - 1 \right]$ so that

$$\mathcal{G}(P) = \frac{1}{\Omega^{m-1}} \sup_{\hat{h}} \left(\mathbb{E}_{P_k} \left[\frac{m}{m-1} \hat{h}^{m-1}(X) \right] - \mathbb{E}_Q \left[\hat{h}^m(Z) \right] \right).$$

With such a change of variable, the optimal function $\hat{h} = T_{\#}^k P_k / Q$.

B Evaluation of the density

In this section, we assume the solving process doesn't use forward-backward scheme, i.e. all the probability measures P_k are obtained by performing JKO one by one. Otherwise, the map $I - a\nabla_x(W * P_k) = I - \mathbb{E}_{y \sim P_k} \nabla_x(W(x-y))$ includes an expectation term and becomes intractable to push-backward particles to compute density.

If T is invertible, there exists a standard approach to evaluate the density of P_k (Alvarez-Melis et al., 2021; Mokrov et al., 2021) through the change of variables formula. More specifically, we assume T is parameterized by the gradient of an ICNN φ that is assumed to be strictly convex. To evaluate the density $P_k(x_k)$ at point x_k , we back propagate through the sequence of maps $T_k = \nabla\varphi_k, \dots, T_1 = \nabla\varphi_1$ to get

$$x_i = T_{i+1}^{-1} \circ T_{i+2}^{-1} \circ \dots \circ T_k^{-1}(x_k).$$

The inverse map $T_j^{-1} = (\nabla\varphi_j)^{-1} = \nabla\varphi_j^*$ can be obtained by solving the convex optimization

$$x_{j-1} = \arg \max_{x \in \mathbb{R}^n} \langle x, x_j \rangle - \varphi_j(x). \quad (15)$$

Then, by the change of variables formula, we obtain

$$\log[P_k(x_k)] = \log[P_0(x_0)] - \sum_{i=1}^k \log |\nabla^2 \varphi_i(x_{i-1})|, \quad (16)$$

where $\nabla^2 \varphi_i(x_{i-1})$ is the Hessian of φ_i and $|\nabla^2 \varphi_i(x_{i-1})|$ is its determinant. By iteratively solving (15) and plugging the resulting x_j into (16), we can recover the density $P_k(x_k)$ at any point.

C Additional experiment results and discussions

C.1 Sampling using ICNN parameterization

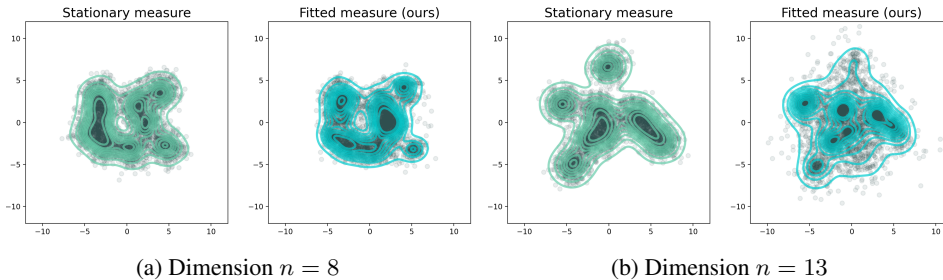


Figure 6: Sampling Gaussian mixture models by parameterizing the map by $\nabla\varphi$.

In Figure 6, we present the sampling results with $\nabla\varphi$ parameterized map where φ is a ICNN neural network. The experiment setting is the same as Section 4.1 and we can observe a MLP network map gives better fitted measures.

C.2 Aggregation equation

Alvarez-Melis et al. (2021) proposes using the neural network based JKO, i.e. the backward method, to solve (17). They parameterize T as the gradient of the ICNN. In this section, we use two cases to compare the forward method and backward when $\mathcal{F}(P) = \mathcal{W}(P)$. This could help explain the FB and non-FB scheme performance difference later in Section C.3.

We study the gradient flow associated with the aggregation equation

$$\partial_t P = \nabla \cdot (P \nabla W * P), \quad W : \mathbb{R}^n \rightarrow \mathbb{R}. \quad (17)$$

The forward method is

$$P_{k+1} := (I - a \nabla_x(W * P_k)) \# P_k.$$

The backward method or JKO is

$$P_{k+1} := T_k \# P_k, \quad T_k = \arg \min_T \left\{ \frac{1}{2a} \mathbb{E}_{P_k} [\|X - T(X)\|^2] + \mathbb{E}_{X, Y \sim P_k} [W(T(X) - T(Y))] \right\}.$$

Example 1 We follow the setting in Carrillo et al. (2021, Section 4.3.1). The interaction kernel is $W(x) = \frac{\|x\|^4}{4} - \frac{\|x\|^2}{2}$, and the initial measure P_0 is a Gaussian $\mathcal{N}(0, 0.25I)$. In this case, $\nabla_x(W * P_k)$ becomes $\mathbb{E}_{y \sim P_k} [(\|x - y\|^2 - 1)(x - y)]$. We use step size $a = 0.05$ for both methods and show the results in Figure 7.

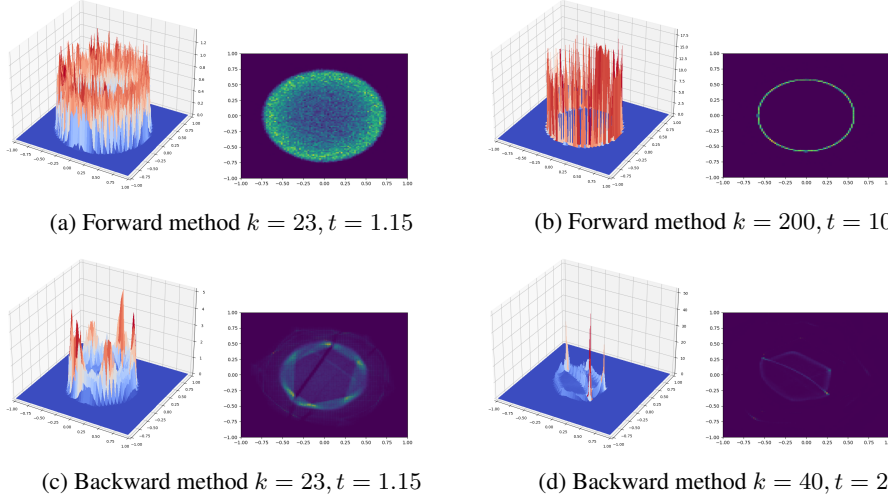


Figure 7: The steady state is supported on a ring of radius 0.5. Backward converges faster to the steady state but is unstable. As k goes large, it cannot keep the regular ring shape and will collapse after $k > 50$.

Example 2 We follow the setting in Carrillo et al. (2021, Section 4.2.3). The interaction kernel is $W(x) = \frac{\|x\|^2}{2} - \ln \|x\|$, and the initial measure P_0 is $\mathcal{N}(0, 1)$. The unique steady state for this case is

$$P_\infty(x) = \frac{1}{\pi} \sqrt{(2 - x^2)_+}.$$

The reader can refer to Alvarez-Melis et al. (2021, Section 5.3) for the backward method performance. As for the forward method, $\nabla_x(W * P_k)$ becomes $\mathbb{E}_{y \sim P_k} \left[x - y - \frac{1}{x-y} \right]$. Because the kernel W enforces repulsion near the origin and P_0 is concentrated around origin, $\nabla_x(W * P)$ will easily blow up. So the forward method is not suitable for this kind of interaction kernel.

Through the above two examples, if $\nabla_x(W * P)$ is smooth, we can notice the backward method converges faster, but is not stable when solving (17). This shed light on the FB and non-FB scheme performance in Section 4.4, C.3. However, if $\nabla_x(W * P)$ has bad modality such as Example 2, the forward method loses the competitiveness.

C.3 Aggregation-diffusion equation with non-FB scheme

In Figure 8, we show the non-FB solutions to Aggregation-diffusion equation in Section 4.4. FB scheme should be independent with the implementation of JKO, but in the following context, we assume FB and non-FB are both neural network based methods discussed in Section 3. Non-FB scheme reads

$$P_{k+1} = T_k \# P_k$$

$$T_k = \arg \min_T \left\{ \frac{1}{2a} \mathbb{E}_{P_k} [\|X - T(X)\|^2] + \mathbb{E}_{X, Y \sim P_k} [W(T(X) - T(Y))] + \mathcal{G}(T, h) \right\},$$

where $\mathcal{G}(T, h)$ is represented by the variational formula (11). We use the same step size $a = 0.5$ and other PDE parameters as in Section 4.4.

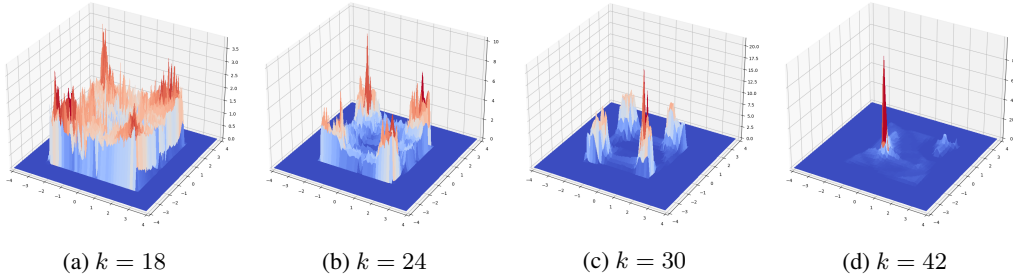


Figure 8: Histograms for simulated measures P_k by non-FB scheme at different k .

Comparing the FB scheme results in Figure 5 and the non-FB scheme results in Figure 8, we observe non-FB converges $1.5\times$ slower than the finite difference method (Carrillo et al., 2021), and FB converges $3\times$ slower than the finite difference method. This may be because splitting one JKO step to the forward-backward two steps removes the aggregation term effect in the JKO, and the diffusion term is too weak to make a difference in the loss. Note at the first several k , both P_k and Q are nearly the same uniform distributions, so h is nearly a constant and $T(x)$ exerts little effect in the variational formula of $\mathcal{G}(P)$. Another possible reason is a single forward step for aggregation term converges slower than integrating aggregation in the backward step, as we discuss in Section C.2 and Figure 7.

However, FB generates more regular measures. We can tell the four pulses given by FB are more symmetric. We speculate this is because gradient descent step in FB utilizes the geometric structure of $W(x)$ directly, but integrating $\mathcal{W}(P)$ in neural network based JKO losses the geometric meaning of $W(x)$.

C.4 Computational time

Our experiments are conducted on GeForce RTX 3090. The forward step (12) takes about 14 seconds to pushforward one million points.

Assume each JKO step involves 500 iterations and the number of inner iteration $J_1 = 3$, then each JKO step (13) takes 100 seconds if the energy function contains the generalized energy $\mathcal{G}(P)$ and 25 seconds if the energy function contains the KL divergence $\mathcal{D}(P||Q)$.

D Implementation details

Our code is written in Pytorch-Lightning (Falcon & Cho, 2020). For some parts of plotting in Section 4.1 and 4.2, we adopt the code given by Mokrov et al. (2021).

Without further specification, we use the following parameters:

- 1) The number of iterations of the outer loop J_1 is 600.
- 2) The number of iterations of the inner loop J_2 is 3.
- 3) The batch size is fixed to be $M = 100$.
- 4) The learning rate is fixed to be 0.001.
- 5) All the activation functions are set to be PReLU.
- 6) h has 4 layers and 16 neurons in each layer.
- 7) T has 5 layers and 16 neurons in each layer.

The transport map T can be parametrized in different ways. We use a residual MLP network for it in Section 4.1, 4.2, C.2 and the gradient of a strongly convex ICNN in Section 4.3, 4.4, C.1, C.3. The dual test function h is always a MLP network with a dropout layer before each layer.

D.1 Sampling (Section 4.1 and C.1)

Two moons We run $K = 10$ JKO steps with $J_2 = 6$ inner iterations. h has 6 layers. T has 5 layers.

GMM 8D example trains for $K = 50$ JKO steps. h has 6 layers and 64 neurons in each layer. T has 3 layers and 128 neurons in each layer.

13D example trains for $K = 20$ JKO steps. h has 8 layers and 64 neurons in each layer. T has 9 layers and 64 neurons in each layer.

D.2 Ornstein-Uhlenbeck Process (Section 4.2)

For Fokker-Planck JKO, we use the implementation provided by the authors and the default parameters given in Mokrov et al. (2021, Section A.2). We also estimate the SymKL using Monte Carlo according to the author’s instructions. It’s straightforward to use MC estimate for Fokker-Planck JKO because it has access to the density of pushforward distributions. Our method uses T parameterization so we cannot query density of the estimated \tilde{P}_t exactly. Nevertheless, our estimated \tilde{P}_t is guaranteed to be a Gaussian distribution since our map T is a linear transformation. Thus we use the density of $\mathcal{N}(\tilde{\mu}_t, \tilde{\Sigma}_t)$ as a surrogate, where $\tilde{\mu}_t, \tilde{\Sigma}_t$ are empirical mean and empirical covariance computed using $5 \cdot 10^5$ samples.

We use nearly all the same hyper-parameters as Mokrov et al. (2021), including learning rate, hidden layer width, and the number of iterations per JKO step. Specifically, we use a linear residual feed-forward NN to work as T , i.e. without activation function. h and T both have 3 layers and 64 hidden neurons per layer for all dimensions. We also train them for $J_1 = 500$ iterations per each JKO with learning rate 0.005. The batch size is $M = 1000$.

D.3 Porous media equation (Section 4.3)

In the experiment, h and T both have 10 neurons in each layer.

To account for the time-discretization error of JKO scheme, we consider the porous media equation in 1D space and use the solution via finite difference method as a reference. More specifically, in the 1D space \mathbb{R} , we discretize the density over a fixed grid with grid size d and grid resolution δx . With this discretization, the probability densities become (scaled) probability vectors and the problem (4) can be converted into a convex optimization

$$\min_{\pi: \delta x \pi^T \mathbf{1} = \hat{P}_k} \frac{(\delta x)^2}{2a} \langle \pi, M \rangle + \frac{\delta x}{m-1} (\mathbf{1}^T \pi \delta x)^m \mathbf{1} \quad (18)$$

where M is the discretized unit transport cost, $\hat{P}_k \in \mathbb{R}^d$ is the probability vector at the previous step, $\mathbf{1} \in \mathbb{R}^d$ is the all-ones vector and the optimization variable $\pi \in \mathbb{R}^d \times \mathbb{R}^d$ is the joint distribution between \hat{P}_k and \hat{P}_{k+1} . This is a standard convex optimization and can be solved with generic solvers. When an optimal π is obtained, \hat{P}_{k+1} can be computed as $\hat{P}_{k+1} = \pi \mathbf{1}$. We adopt the library CVXOPT¹ to solve the convex programming problem (18). In so doing, we arrive at a reference solution $\hat{P}_0, \hat{P}_1, \dots, \hat{P}_k, \dots$ for our algorithm.

D.4 Aggregation-diffusion equation (Section 4.4 and C.3)

Each JKO step contains $J_1 = 200$ iterations. The batch size is $M = 1000$.

¹<http://cvxr.com/cvx/>